Analysis, Design, and Implementation of a Quasi-Proportional-Resonant Controller for a Multifunctional Capacitive-Coupling Grid-Connected Inverter

Tao Ye, NingYi Dai, *Senior Member, IEEE*, Chi-Seng Lam, *Senior Member, IEEE*, Man-Chung Wong, *Senior Member, IEEE*, and Josep M. Guerrero, *Fellow, IEEE*

***Abstract*—The capacitive-coupling grid-connected inverter (CGCI) is coupled to the point of common coupling via a second-order *LC* branch. Its operational voltage is much lower than that of a conventional inductive-coupling grid-connected inverter (IGCI) when it serves as a multifunctional inverter to compensate reactive power and transfer active power simultaneously. It is a promising solution for microgrid and building-integrated distributed generator systems. A quasi-proportional-resonant (quasi-PR) controller is applied to reduce the steady-state current tracking errors of the CGCI in this paper. The quasi-PR controller generates the voltage reference for use of carrier-based pulse-width modulation, which can effectively reduce output current ripples. The second-order coupling impedance of the CGCI causes its modeling and controller design to differ from that of the conventional IGCI. A comprehensive design method for the quasi-PR controller in a CGCI is developed. The quasi-PR controller is also compared with a proportional-integration current controller. Simulation results are provided to verify the effectiveness of the quasi-PR controller and its design method in a CGCI. The current tracking errors are greatly reduced when the quasi-PR controller rather than the proportional-integration controller is applied. Experimental results are also provided to validate the CGCI as a multifunctional grid-connected inverter.**

***Index Terms*—Active power, capacitive-coupling grid-connected inverter (CGCI), proportional-integration controller, quasi-proportional-resonant (PR) controller, reactive power.**

Manuscript received October 21, 2015; revised February 5, 2016 and April 13, 2016; accepted May 25, 2016. Date of publication June 15, 2016; date of current version September 16, 2016. Paper 2015-SECSC-0826.R2, presented at the 2015 IEEE Energy Conversion Congress and Exposition, Montreal, QC, Canada, Sep. 20–24, and approved for publication in the IEEE TRANSACTIONS ON INDUSTRY APPLICATIONS by the Sustainable Energy Conversion Systems Committee of the IEEE Industry Applications Society. This work was supported by the Science and Technology Development Fund, Macao SAR Government, under Project 072/2012/A3, and by the University of Macau under Project MRG014/DNY/2013/FST and Project MYRG2015-00084-FST.

T. Ye and N. Dai are with the Electrical and Computer Engineering Department, University of Macau, Macau, China (e-mail: wkderic@126.com; nydai@umac.mo).

C.-S. Lam is with the State Key Laboratory of Analog and Mixed-Signal VLSI, University of Macau, Macau, China (e-mail: cslam@umac.mo).

M.-C. Wong is with the Department of Electrical and Computer Engineering, and the State Key Laboratory of Analog and Mixed-Signal VLSI, University of Macau, Macau, China (e-mail: mcwong@umac.mo).

J. M. Guerrero is with the Department of Energy Technology, Aalborg University, Aalborg 9100, Denmark (e-mail: joz@et.aau.dk).

Color versions of one or more of the figures in this paper are available online at http://ieeexplore.ieee.org.

Digital Object Identifier 10.1109/TIA.2016.2581152

I. INTRODUCTION

THE INCREASING need for more effective and environmentally friendly electrical power systems plays an important role in the development of a smart grid [1]–[4]. The grid-connected inverter is the key element for efficient use of distributed energy resources. Recently, increasing attention has been paid to multifunctional grid-connected inverters, which can provide auxiliary services to enhance power quality [5], [6] in addition to providing active power transfer. Previous research on grid-connected inverters has mainly used an *LC*-type or *LCL*-type filter to reduce output current distortion [7], [8]. This type of grid-connected inverter is called an inductive-coupling grid-connected inverter (IGCI) in this paper because the fundamental frequency coupling impedance is inductive [9]–[11]. The IGCI usually requires a high dc-link voltage because its operational voltage should be higher than the grid voltage to transfer active power and perform power quality conditioning.

A capacitive-coupling grid-connected inverter (CGCI) was also proposed [12], [13].The CGCI is coupled to the grid via an inductor in series with a capacitor. The fundamental frequency impedance of its coupling branch is capacitive. This topology was first proposed under the name of hybrid filter [14]–[17], and it has shown its advantage in reducing operational voltage under certain circumstances. The CGCI can transfer active power and inject leading reactive power into a grid with an operational voltage lower than the grid voltage [17]–[21]. The required dc-link voltage is much lower than that of the IGCI. As a result, the CGCI appears to be a promising solution for building-integrated photovoltaic generation systems or small-scale microgrids. It can be coupled to a low-voltage dc bus to provide reactive power and inject active power into an ac grid.

As aforementioned, the capacitive-coupling inverter was first named as hybrid active power filter (HAPF) and was used to damp harmonic resonance in industrial power system [14]–[17]. The inverter output voltage reference is obtained by amplifying harmonic current by a gain *K*. Then carrier-based pulse-width modulation (PWM) or space vector modulation is used. The following study was concerned with the fundamental frequency reactive power control capability of the HAPF. Since the previous voltage reference is not applicable, current tracking directly with hysteresis PWM was adopted to control the *LC*-HAPF [18]–[21]. This method is simple and easy to implement.

However, the sampling rate for the current must be high enough to track the reference current accurately. At the same time, the hysteresis PWM method has the drawbacks of widely varying switching frequency and large current ripples. The carrier-based PWM can fix the variability of switching frequency and reduce output current distortion. However, a voltage reference needs to be generated for controlling the CGCI, so it can use carrier-based PWM [6], [7], [10], [11], [22]–[24].

A current controller could convert current reference to voltage reference. The proportional (*P*) current controller was used to derive the voltage reference in CGCI [12]. A *P-unit* current controller was proposed for the CGCI [13], which is equivalent to a proportional (P) controller in the *s*-domain and is equivalent to a proportional-integral (PI) controller in the z-domain. A high gain must be used to guarantee the performance of the current controller, which does not meet stability margin requirements. In addition, the parameters are selected by trying and testing. Hence, a current controller with better performance should be applied.

PI and proportional-resonant (PR) controllers are the two most widely used current controllers for IGCI [6]–[11], [24]–[28]. The conventional PI controller is not capable of eliminating steady-state errors in current tracking [9], [22], [24], [29], especially when an *LC* or *LCL* filter is coupled to the inverter. A synchronous PI controller was proposed to achieve theoretical zero steady-state errors for a three-phase inverter, in which stationary frame ac quantities are transformed to dc quantities [22], [30]. However, additional computations are required to coordinate the transformation when this method is applied to the single-phase IGCI. A stationary-frame PR controller has the same operational principle as a synchronous-frame PI controller when it is applied to the conventional single-phase IGCI [22], [31], [32]. Compared to the stationary-frame PR controller, a quasi-PR controller can avoid the stability problems associated with an infinite gain and reduce the sensitivity toward slight frequency variation [31], [33].

Sliding mode control (SMC) can provide attractive features such as fast transient response and applicable to multivariable systems. But its chattering problems may lead to low steady-state accuracy, especially when switching frequency is not high enough [34]–[37]. Repetitive control (RC) can be employed to improve tracking accuracy by placing an internal model into the loop. The dynamic response of RC is much slower than that of a feedback controller such as PI or PR controller [38], [39]. Many other advanced controllers have been proposed, such as adaptive SMC, improved RC, model predictive control, fuzzy logic control (FLC), and artificial neural network control (ANNC) [40]–[44]. These control methods could be more robust under system parameter variations and could achieve fast transient response. However, more efforts are required to implement these controllers. It is a time-consuming task to realize them on a digital controller using C/C++ language. What's more, the performance of adaptive-based control, FLC, and ANNC are also related to the available training data.

As the first step to improve the current controller of the CGCI, a quasi-PR current controller is applied to control the CGCI for the first time, which can achieve zero steady-state error at the selected oscillation frequency with relatively small gain. The second-order coupling impedance of the CGCI causes its control model to differ from that of the conventional IGCI. The system response after applying the quasi-PR controller to the CGCI will be studied for parameter selection, which has not been done before. A comprehensive design method for the quasi-PR controller will also be developed.

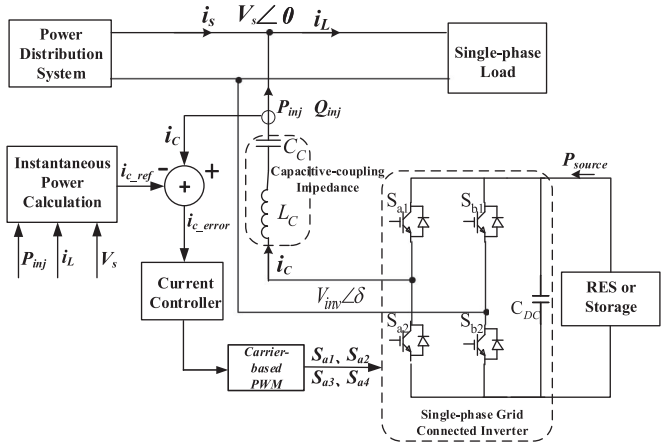

Fig. 1. Circuit configuration of a single-phase CGCI.

The operational principle of the CGCI is briefly introduced in Section II, followed by the mathematical model of its current control loop. The design of the quasi-PR controller for a CGCI is presented in Section III, in which a comparison with the PI current controller is also given. Simulation results for a CGCI with the quasi-PR controller are given for comparison with those with the PI controller in Section IV. The experimental results are provided in Section V. Finally, conclusion is drawn in Section VI.

II. Modeling of the CGCI

A. Operational Principle of the CGCI

The circuit configuration of a single-phase CGCI is shown in Fig. 1, where v_s and $V_{\rm inv}$ denote grid voltage and inverter output voltage, and i_s, i_L and i_c are source, load, and compensating currents, respectively. L_c and C_c are the coupling inductor and capacitor, respectively, and $C_{\rm dc}$ is the dc-link capacitor.

The power flow ($P_{\rm inj}$ and $Q_{\rm inj}$) between the voltage source inverter and the grid can be calculated as follows [45]:

$$P_{\rm inj} = \left(\frac{V_s V_{\rm inv}}{Z}\cos\delta - \frac{V_s^2}{Z}\right)\cos\theta + \frac{V_s V_{\rm inv}}{Z}\sin\delta\sin\theta \quad (1)$$

$$Q_{\rm inj} = \left(\frac{V_s V_{\rm inv}}{Z}\cos\delta - \frac{V_s^2}{Z}\right)\sin\theta - \frac{V_s V_{\rm inv}}{Z}\sin\delta\cos\theta. \quad (2)$$

In (1) and (2), δ represents the phase angle between V_s and $V_{\rm inv}$. The values of Z and θ are determined by the coupling impedance of the grid-connected inverter, which can be

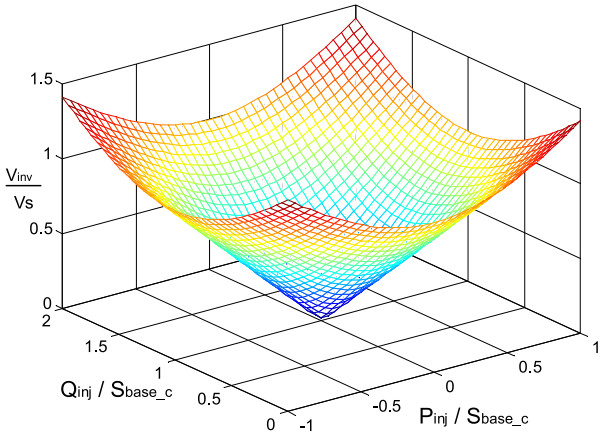

Fig. 2. Inverter output voltage versus active and reactive power flow.

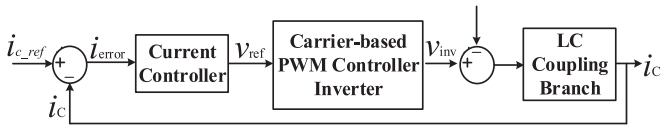

Fig. 3. Current control loop block diagram of the CGCI.

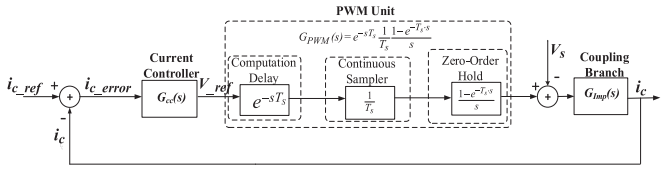

Fig. 4. S-domain model of the current control loop of the CGCI.

expressed as

$$X_c = Z\angle\theta = -j\frac{1}{\omega C_c} + j\omega L_c = -j\frac{1}{\omega C} = \frac{1}{\omega C}\angle -90^\circ. \tag{3}$$

The power base is introduced as follows:

$$S_{\text{base}} = V_s^2 \cdot \omega C. \tag{4}$$

By combining (1)–(4), the normalized output voltage of the CGCI is calculated as in (5), and its variation in normalized power flow can be plotted in three dimensions as shown in Fig. 2

$$\frac{V_{\text{inv}}}{V_s} = \sqrt{\left(\frac{P_{\text{inj}}}{S_{\text{base}}}\right)^2 + \left(\frac{Q_{\text{inj}}}{S_{\text{base}}} - 1\right)^2}. \tag{5}$$

According to analyses in previous works [12], [13], the inverter operational voltage is lower when its output reactive power varies in the vicinity of S_{base}. Thus, it is better to connect the CGCI to the point of common coupling (PCC), at which continuous reactive power compensation is required for inductive loadings such as in water pumps, centralized air-conditioning systems, etc. Under this situation, the CGCI can simultaneously inject active power from a distributed source to the grid while keeping its operational voltage low.

When the CGCI is used to transfer active power from the renewable energy sources and compensate reactive power at the PCC simultaneously, the output current reference is calculated as follows:

$$i_{c\_\text{ref}} = \frac{1}{v_m^2}\begin{bmatrix}\sin\theta & \cos\theta\end{bmatrix}\begin{bmatrix}P_{\text{source}} \\ q_L\end{bmatrix} \tag{6}$$

where P_{source} represents the active power from distributed generators. q_L is the load reactive power extracted by using the instantaneous reactive power theory [12], [13].

B. Modeling the Current Control Loop of the CGCI

A current control loop is adopted to control the output current of the CGCI to track the current reference, as illustrated in Fig. 3. The carrier-based PWM method is used. Its corresponding mathematical model is deduced as given in Fig. 4.

The mathematical model of each block in Fig. 4 is as follows.

1. Current Controller: $G_{\text{cc}}(\text{s})$ As mentioned in the previous section, current controllers with different characteristics have been developed for conventional grid-connected inverters, which are coupled to the grid via inductive impedance. A current control is designed for controlling the CGCI, which is analyzed in detail in the next section.

2. PWM Unit: $G_{\text{PWM}}(\text{s})$ In an average s-domain model, the PWM converter can be simplified to a unity gain. However, the computation time of the digital controller cannot be negligible [9], [46]–[48]. To accurately describe the effects of time delay on the CGCI controller, the computation delay, sampler, and zero-order hold as an s-domain PWM unit model are used as shown in Fig. 4. The s-domain transfer function of the PWM unit can be expressed as

$$G_{\text{PWM}}(s) = \frac{e^{-T_s\cdot s}(1 - e^{-T_s\cdot s})}{T_s \cdot s} \tag{7}$$

where T_s is the sampling period. To accurately reveal digital implementation effects and obtain a rational transfer function, delays are usually approximated by poles and zeros [49]–[52]. A proper way to accomplish this is to use the $Pade'$ approximation. The first-order $Pade'$approximation shown in (8) can maintain the s-domain analysis with fair agreement between simplicity and accuracy

$$e^{-T_s\cdot s} \approx \frac{1 - 0.5\cdot T_s\cdot s}{1 + 0.5\cdot T_s\cdot s} = Pade'. \tag{8}$$

Substituting (8) into (7) yields

$$G_{\text{PWM}}(s) = \frac{e^{-T_s\cdot s}(1 - e^{-T_s\cdot s})}{T_s\cdot s} \approx \frac{1 - 0.5\cdot T_s\cdot s}{(1 + 0.5\cdot T_s\cdot s)^2}. \tag{9}$$

3. Coupling Impedance: $G_{\text{Imp}}(s)$ The *LC* coupling branch of the CGCI can be expressed as

$$G_{\text{Imp}}(s) = \frac{C_c s}{L_c C_c s^2 + 1}. \tag{10}$$

According to Fig. 4, the overall transfer function of the CGCI controller is obtained as

$$\begin{aligned} I_c(s) =& \; G_{\mathrm{cref\_}c} I_{c\_\mathrm{ref}}(s) - G_{vs\_c} V_S(s) \\ =& \; \frac{G_{cc}(s) G_{\mathrm{PWM}}(s) G_{\mathrm{Imp}}(s)}{1 + G_{cc} G_{\mathrm{PWM}}(s) G_{\mathrm{Imp}}(s)} I_{c\_\mathrm{ref}}(s) \\ & - \frac{G_{\mathrm{Imp}}(s)}{1 + G_{cc} G_{\mathrm{PWM}}(s) G_{\mathrm{Imp}}(s)} V_S(s) \end{aligned} \tag{11}$$

where $G_{\mathrm{cref\_}c}(s)$ is the system closed-loop transfer function between i_c and i_{c_ref}, and $G_{vs\_ic}(s)$ is the closed-loop system transfer function between i_c and V_s. $G_{\mathrm{Quasi-PR}}(s)$ $G_{\mathrm{PWM}}(s) G_{\mathrm{Imp}}(s)$ is the open-loop transfer function.

III. Design of a Quasi-PR Controller for the CGCI

A. Quasi-PR Controller for the CGCI

A quasi-PR controller is used as the current controller in Fig. 4. Its transfer function is expressed as

$$G_{cc}(s) = G_{\mathrm{Quasi-PR}}(s) = K_p + \frac{2K_r \omega_c s}{s^2 + 2\omega_c s + {\omega_0}^2}. \tag{12}$$

Three parameters need to be selected for a quasi-PR current controller to simplify the parameters tuning procedure. The typical design scenario can be summarized as follows.

1) An appropriate ω_c should be chosen to give a satisfactory bandwidth around the resonant frequency.
2) K_p should be chosen such that good transient response and stability are guaranteed.
3) K_r is chosen so that phase and magnitude steady-state errors are eliminated.

On the basis of the power quality standards of Macau and Hong Kong (CEM supply rules, HKE and CLP supply rules of Hong Kong), the standard limit of frequency variation is $\pm 2\%$ [57], [58]. Assuming that the frequency variation margin is $\pm 2\%$, then ω_c can be designed as $\omega_c = 2 * \pi * 50 * 2\% = 6.28$.

K_p should be high enough to obtain high gain at the fundamental frequency and the low-order harmonic frequency. However, the stability margin may be sacrificed when the K_p value is increased. The boundary of the K_p value is determined by using Routh's stability criterion. The open-loop transfer function of the related closed-loop transfer function $G_{\mathrm{cref\_}c}(s)$ is $G_{\mathrm{Quasi-PR}}(s) G_{\mathrm{PWM}}(s) G_{\mathrm{Imp}}(s)$ and assume that $G_{\mathrm{cref\_}c}(s) = N(s)/D(s)$. Then, the characteristic equation can be obtained

$$D(s) + KN(s) = 0 \tag{13}$$

where K indicates the upper boundary of the proportional gain under different K_p values. It is assumed that the delay time of the PWM unit is just half of the sampling period ($0.5T_s$); then, the corresponding boundary of K_p can be deduced as follows:

$$K_p \leq \frac{8 \cdot L_c}{3 \cdot T_s}. \tag{14}$$

The value of K_r is adjusted to limit the steady-state error. For example, the magnitude of $G_{\mathrm{Quasi-PR}}(s) G_{\mathrm{PWM}}(s) G_{\mathrm{Imp}}(s)$ needs to be higher than 100 to decrease the current tracking error to less than 1% according to (11) and without considering the effect of grid-side voltage V_s. Both K_r and K_p are adjusted to satisfy this requirement and simultaneously guarantee enough stability margin.

TABLE I
Selected Parameters for MATLAB Simulation

	Parameters	Value
System settings	Switching frequency f_s	10 kHz
	Fundamental frequency	50 Hz
	Filter inductor L_C	4 mH
	Filter capacitor C_C	125 μF
Quasi-PR controller	$K_r = 5800; K_p = 50; \omega_c = 6.28;$	
PI controller	$K_p = 72; K_i = 4200$	
PR controller	$K_r = 5800; K_p = 50;$	

In summary, the design procedures of the quasi-PR controller for a CGCI are as follows.

1) According to the power quality standard, select the value of ω_c

$$\omega_c = 2 \cdot \pi \cdot f_0 \cdot \Delta f \tag{15}$$

where f_0 is the fundamental frequency, and Δf is the standard limit of the frequency variation.
2) Calculate the upper boundary of the controller's proportional gain K_p according to (14). Select a value of K_p within this boundary.
3) Set a small value for K_r, which can guarantee that the magnitude response of the open-loop transfer function at the designed resonant frequency (50 Hz), is above 40 dB.
4) Adjust the K_p value within its boundary so that the magnitude response of closed-loop transfer function $G_{\mathrm{cref\_}c(s)}$ approaches 0 dB and its phase response approaches 0° at the fundamental frequency. Meanwhile, the frequency response of $G_{\mathrm{cref\_}c(s)}$ should provide adequate attenuation of any high-frequency interference signal.
5) The value of K_r is adjusted to ensure that the magnitude response of $G_{\mathrm{cref\_}c(s)}$ at high frequencies, especially around 10 KHz, is well suppressed.
6) The magnitude response of the closed-loop transfer function $G_{vs\_c(s)}$ is evaluated to guarantee enough attenuation to the grid-side voltage disturbances.

B. Design Verification of the Parameters

The model of the current control loop is analyzed by using MATLAB. The system parameter settings of the CGCI are given in Table I. According to (14), the K_p value should be smaller than 106. The selected parameters for the quasi-PR controller and the PI controller are also listed in Table I. Bode diagrams of the open-loop and closed-loop current control systems are shown in Figs. 5 and 6, respectively.

It can be concluded from Fig. 5 that the open-loop gain at the designed resonant frequency (50 Hz) is above 40 dB. Hence, the closed-loop response of $G_{\mathrm{cref\_}c}(s)$ achieves unity gain with zero phase shifting at the designed resonant frequency. To illustrate

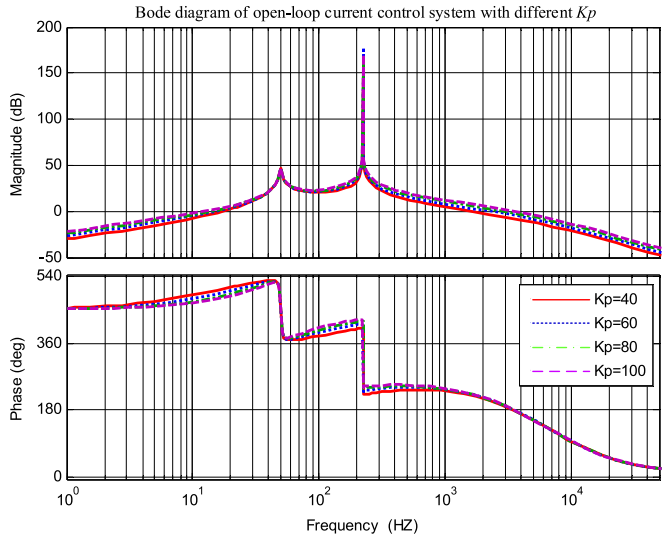

Fig. 5. Bode diagram of the open-loop current control system– $G_{\mathrm{Quasi-PR}}(s)G_{\mathrm{PWM}}(s)G_{\mathrm{Imp}}(s)$ with $\omega_c = 5, K_r = 5000$ and different K_p.

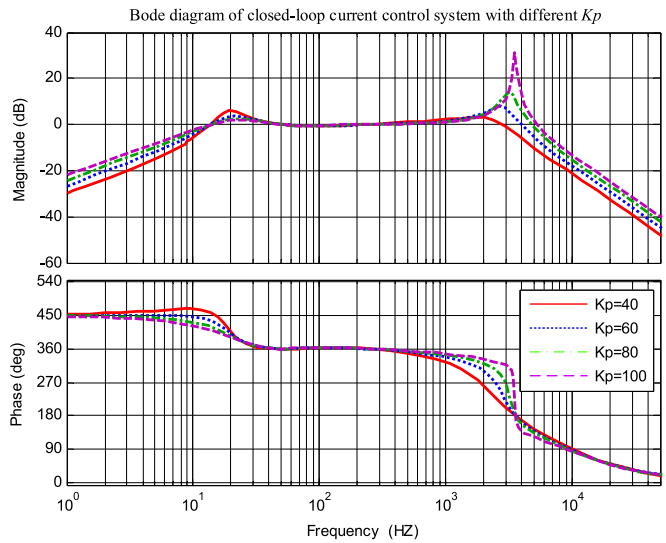

Fig. 6. Bode diagram of the closed-loop current control system –$G_{\mathrm{cref\_c}}(s)$ with $\omega_{\mathrm{c}} = 5, \mathrm{K_r} = 5000$ and different K_p.

the effect of K_p on the frequency response, curves obtained by using four different K_p values are shown in Figs. 5 and 6. In case the stability margin can be satisfied, a higher K_p results in good current tracking performance at the fundamental frequency response. However, to attenuate the high-frequency interference signal simultaneously, a K_p value of around 60 is a better choice according to Fig. 6.

The Bode diagram of closed-loop transfer function $G_{vs\_c}(s)$ is shown in Fig. 7. The results indicate that the designed current control loop with the quasi-PR controller provides enough attenuation to the disturbance from the grid-side voltage. That is, the distortion component in the grid-side voltage will not be

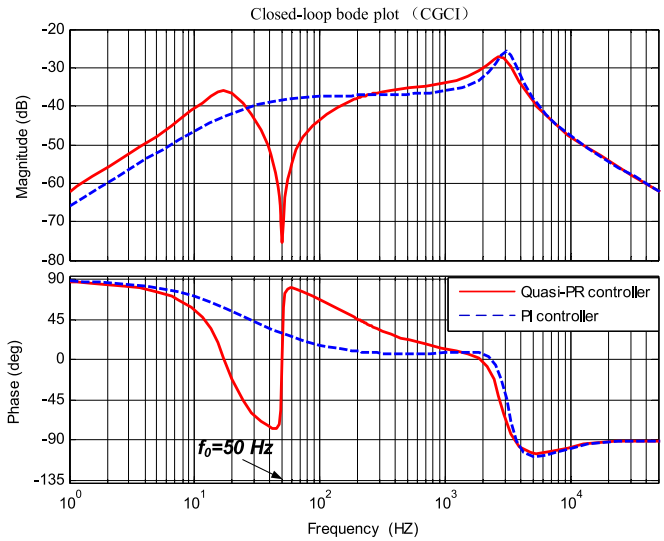

Fig. 7. Bode diagram of the closed-loop transfer functions $G_{\mathrm{vs_c}}(s)$ (solid line: Quasi-PR controller; dashed line: PI controller).

amplified by the CGCI, even though its coupling circuit is a second-order *LC* branch.

C. Comparison Between the PI Controller and Quasi-PR Controller

In this section, a comparison between application of the PI controller and the quasi-PR controller to CGCI is performed. The PI controller is expressed as follows:

$$G_{cc}(s) = G_{\mathrm{PI}}(s) = K_p + \frac{K_i}{s}. \tag{16}$$

By substituting (16) as the current controller into (11), the s-domain closed-loop transfer function with the PI controller is obtained. The system parameters of this controller are listed in Table I. The Bode diagram of $G_{vs\_c}(s)$ is also shown in Fig. 7 when PI controller is adopted. This controller also provides good attenuation of the grid voltage disturbances.

The Bode diagram of $G_{\mathrm{cref\_c}}(s)$ by using the PI controller and quasi-PR controller is shown in Fig. 8. A zoomed view of this figure in the vicinity of the fundamental frequency is shown in Fig. 9. The current tracking error is clearly reduced when the quasi-PR controller is used, especially at the fundamental frequency. Increasing the K_p of the PI controller may force the magnitude response to approach zero. However, a large gain could cause the control system to become unstable and weaken its capability to attenuate high-frequency interference signals. The quasi-PR control uses a lower K_p value, which meets the aforementioned stability margin requirement and design criterion.

D. Comparison Between the PR Controller and the Quasi-PR Controller

In this section, a study is carried out to compare the PR controller and the quasi-PR controller. Both of these two controllers

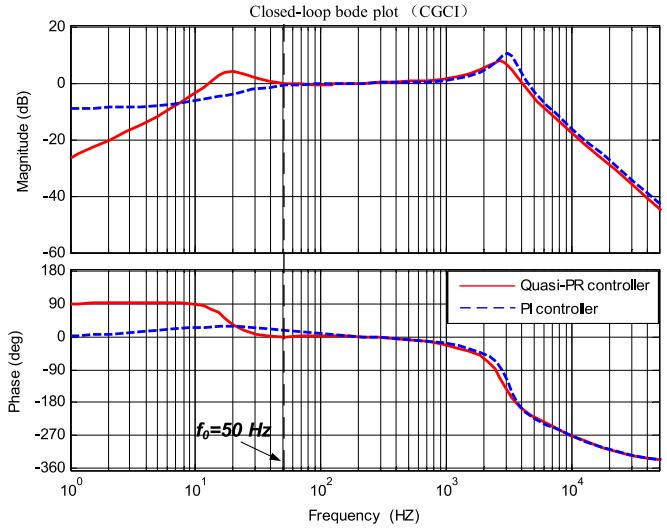

Fig. 8. Bode diagram of the closed-loop transfer function $G_{\mathrm{cref_c}}(\mathrm{s})$ (solid line: Quasi-PR controller; dashed line: PI controller).

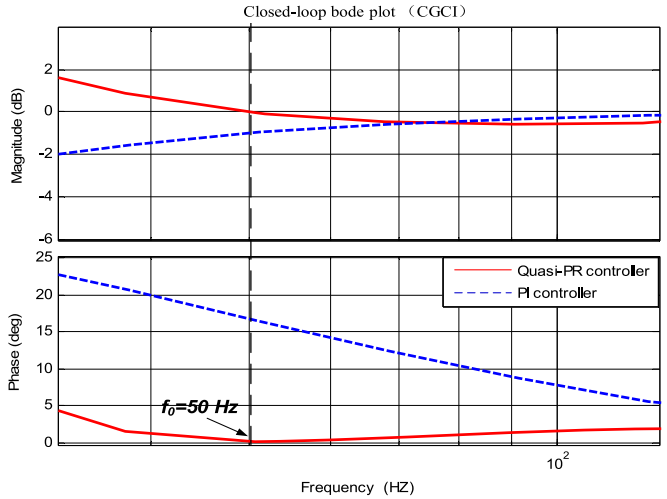

Fig. 9. Zoomed view of Fig. 8.

have not been applied to CGCI in early work. A PR controller is expressed as follows:

$$G_{cc}(s) = G_{\mathrm{PR}}(s) = K_p + \frac{2K_r s}{s^2 + {\omega_0}^2}. \tag{17}$$

The system parameters of the PR controller are listed in Table I. The coefficient K_p and K_r are set to the same value as that of the quasi-PR controller. The Bode diagram of the open-loop current control system with the PR controller and the quasi-PR controller is shown in Fig. 10. It can be concluded that a PR controller introduces an infinite gain at the system frequency (50 Hz). The gain of the quasi-PR controller is finite, but still relatively high for reducing steady-state error. In addition, the bandwidth of the quasi-PR controller can be widened by adjusting the parameter ω_c, so that the sensitivity toward slight frequency variation in a utility grid is reduced [53]–[56].

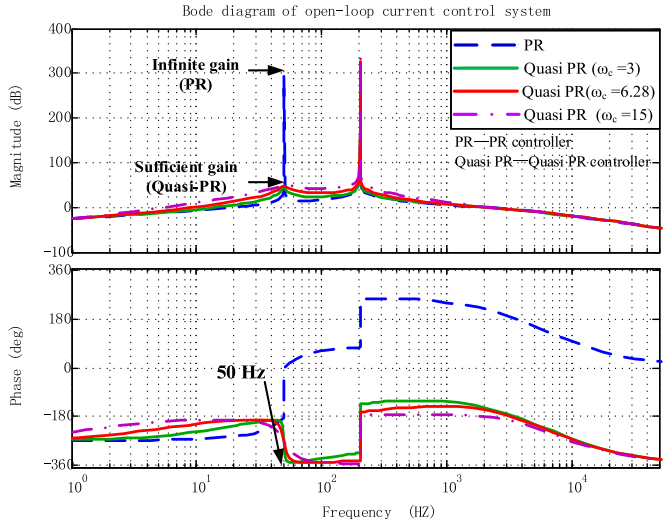

Fig. 10. Bode diagram of the open-loop current control system.

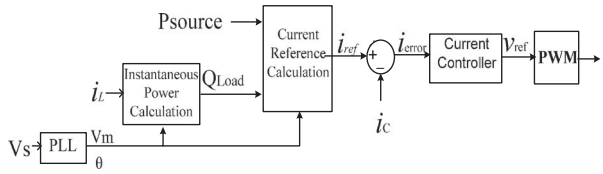

Fig. 11. Control block diagram of the CGCI.

TABLE II
SYSTEM PARAMETER SETTINGS IN THE SIMULATION

System parameters	
Grid parameters	**Value**
Grid voltage V_s	220 V
Fundamental frequency f_0	50 Hz
Sampling frequency	20 kHz
Source inductor L_s	0.001 mH
Inverter parameters	**Value**
DC-link capacitor C_{DC}	1 mF
Filter inductor L_c	4 mH
Filter capacitor C_c	125 μF
Linear load ('//': parallel structure; '+': cascaded structure)	
DC-link voltage V_{DC}	170 V
Linear load 1 (0.5–0.7 s)	15 Ω // (120 mH + 8 Ω)
Linear load 2 (0.1–0.3 s)	20 Ω // (6 mH + 10 Ω)
Linear load 3 (0.3–0.5 s)	28 Ω // (4 mH + 8 Ω)

IV. SIMULATION RESULTS

A. Simulation Setting

To verify the effectiveness of the quasi-PR controller for the CGCI, a set of simulation tests is carried out by using PSCAD/EMTDC. The control block diagram is shown in Fig. 11. Table II lists the simulated system parameters, in which the dc-link voltage of the inverter is supplied by an ideal dc voltage source. The CGCI simultaneously injects active power from the external sources into the grid and compensates reactive

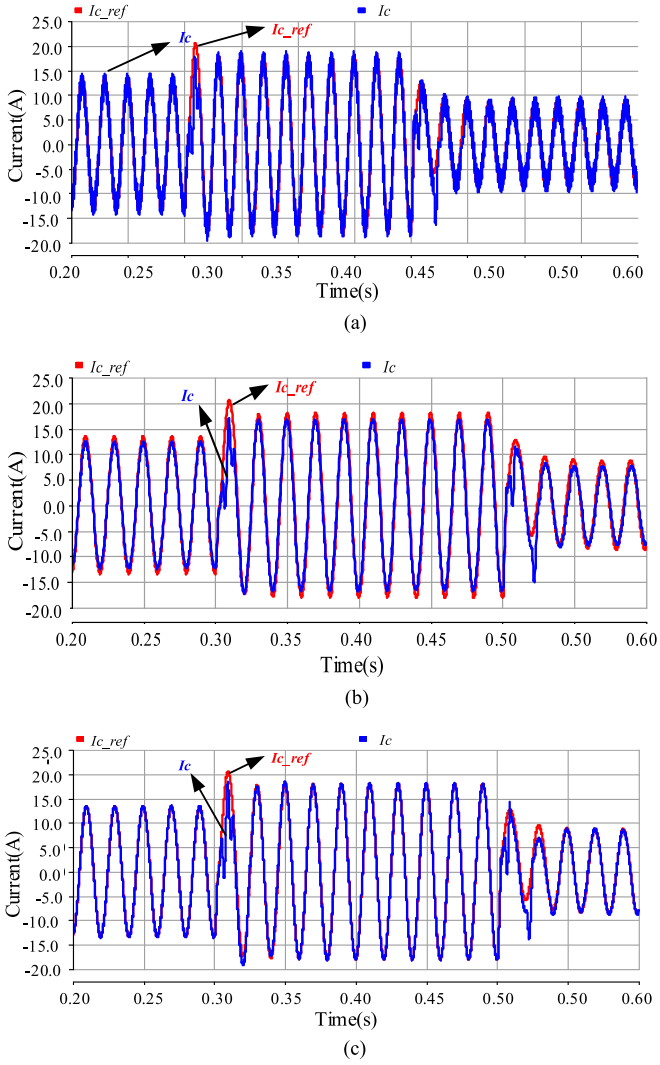

Fig. 12. Current tracking waveforms. (a) Hysterisis band controller. (b) PI controller. (c) Quasi-PR controller.

power of the loads. The dc-link voltage is lower than the grid voltage when the CGCI is used.

The comparison mainly focuses on the steady-state performance. Thus, the performances are conducted with respect to the following parameters.

1) Source current total harmonic distortion (THD) at the steady-state situation.
2) Active power error

$$P_{\text{\_error}} = \left|P_{\text{source}} - P_{\text{\_inj}}\right| / P_{\text{source}} \tag{18}$$

where $P_{\text{\_inj}}$ is the output active power of the CGCI, and P_{source} is the active power reference, which is set in the simulation to model the output of the external sources.

3) Reactive power error

$$Q_{\text{\_error}} = \left|Q_{\text{\_Load}} - Q_{\text{\_inj}}\right| / Q_{\text{\_Load}} \tag{19}$$

where $Q_{\text{\_inj}}$ is the output reactive power of the CGCI and $Q_{\text{\_load}}$ is the reactive power of loads connected to the PCC.

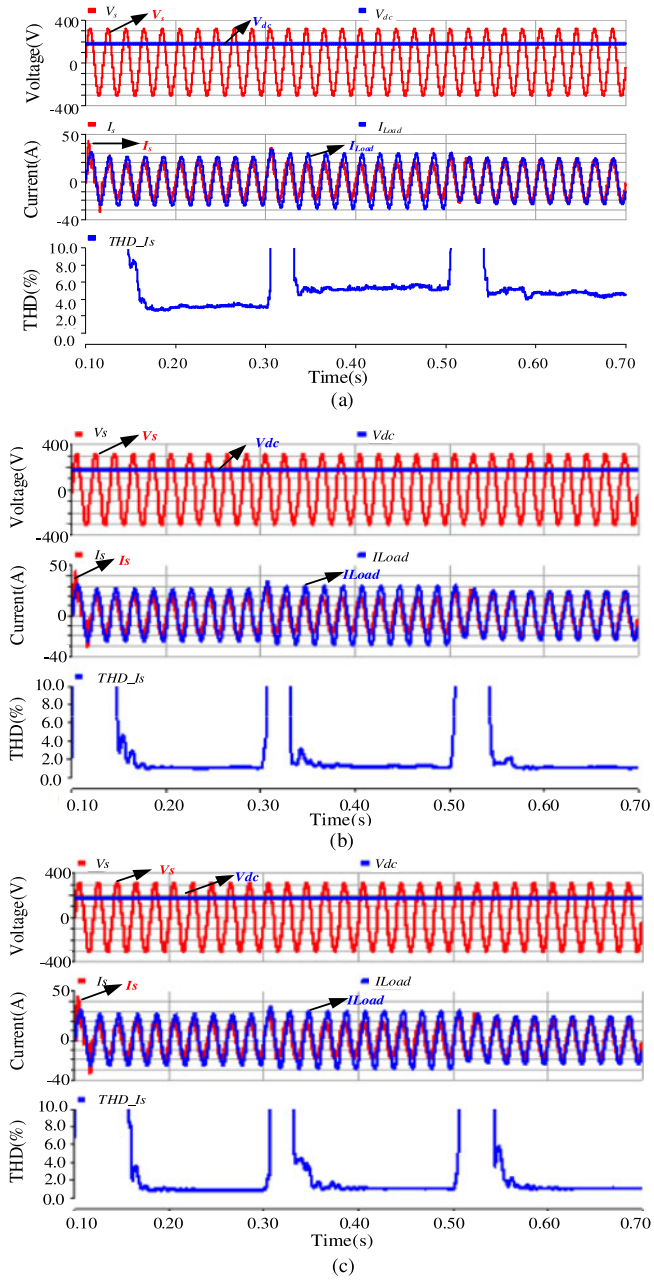

Fig. 13. Voltage and current waveforms and source current THD. (a) Hysterisis band control. (b) PI controller. (c) Quasi-PR controller.

B. Comparisons of Steady-State Performance

The quasi-PR controller is used as the current controller to generate a reference voltage for the carrier-based PWM. In order to illustrate the effectiveness of the quasi-PR controller in reducing steady-state current tracking error, the hysteresis band controller [18], [19] and PI controller are also used in the simulation. The hysteresis band controller could directly control the output current of the inverter to track its reference. Simulation results are shown in Figs. 12–14, respectively. The current reference and output current of the CGCI are shown in Fig. 12. Voltage and

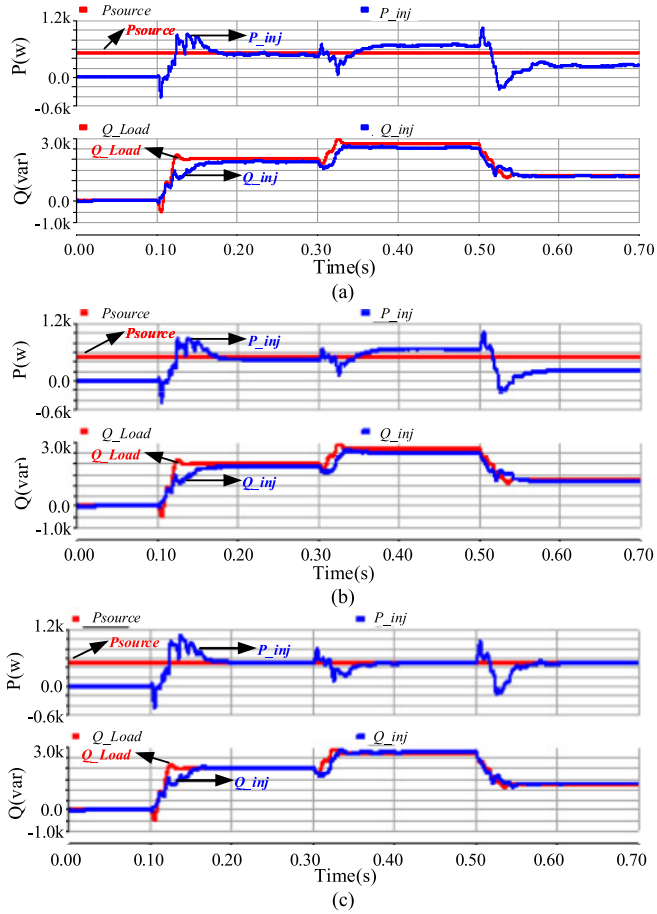

Fig. 14. Active power and reactive power. (a) Hysterisis band controller. (b) PI controller. (c) Quasi-PR controller.

TABLE III
STEADY-STATE PERFORMANCE USING HYSTERESIS BAND CONTROLLER

Hysterisis band control							
Time	THD_is (%)	$P_{\_inj}$ (W)	P_{source} (W)	$Q_{\_inj}$ (var)	$Q_{\_load}$ (var)	$P_{\_error}$ (%)	$Q_{\_error}$ (%)
0.29 s	3.02	447.50	500	1879.24	2002.3	10.5	6.15
0.49 s	4.99	646.91	500	2548.65	2738.78	29.38	6.94
0.69 s	4.53	260.08	500	1157.7	1227.64	47.98	5.70

current waveforms and *THD_is* variations are shown in Fig. 13. The active power and reactive power variations are provided in Fig. 14.

The system performance indexes at the steady state are summarized in Tables III–V. It can be concluded that the current tracking error is reduced by using the quasi-PR controller. The hysteresis band controller and the PI controller cannot eliminate the steady-state current tracking errors. A similar case also occurs when the PI controller is applied to control an IGCI [6], [9], [11], [22], [25]–[27], [31]. As a result, both the active and reactive power outputs of the CGCI cannot track the reference with high accuracy. When the quasi-PR controller is used, however, both the active and reactive power tracking errors are lower.

TABLE IV
STEADY-STATE PERFORMANCE USING THE PI CONTROLLER

PI controller ($K_p = 72, K_i = 4500$)							
Time	THD_is (%)	$P_{\_inj}$ (W)	P_{source} (W)	$Q_{\_inj}$ (var)	$Q_{\_load}$ (var)	$P_{\_error}$ (%)	$Q_{\_error}$ (%)
0.29 s	0.95	439.39	500	1855.86	2002.29	12.12	7.31
0.49 s	1.09	659.07	500	2510.47	2738.77	31.81	8.34
0.69 s	1.10	214.17	500	1178.07	1227.64	57.17	4.04

TABLE V
STEADY-STATE PERFORMANCE USING THE QUASI-PR CONTROLLER

Quasi-PR controller ($K_p = 50, \omega_c = 6.28, K_r = 5800$							
Time	THD_is (%)	$P_{\_inj}$ (W)	P_{source} (W)	$Q_{\_inj}$ (var)	$Q_{\_load}$ (var)	$P_{\_error}$ (%)	$Q_{\_error}$ (%)
0.29 s	0.84	500.12	500	2021.64	2002.3	0.02	0.97
0.49 s	0.99	499.94	500	2761.53	2738.78	0.01	0.83
0.69 s	1.02	482.22	500	1257.3	1227.64	3.56	2.42

TABLE VI
STEADY-STATE PERFORMANCE USING THE PR CONTROLLER WHEN SYSTEM FREQUENCY IS 49.1 HZ

Time	THD_is (%)	$P_{\_inj}$ (W)	P_{source} (W)	$Q_{\_inj}$ (var)	$Q_{\_load}$ (var)	$P_{\_error}$ (%)	$Q_{\_error}$ (%)
0.29 s	2.43	495.28	500	2086.63	2020.23	0.94	3.29
0.49 s	4.52	539.52	500	2834.38	2756.35	7.90	2.83
0.69 s	2.84	474.84	500	1309.52	1246.72	5.03	5.04

TABLE VII
STEADY-STATE PERFORMANCE USING THE QUASI-PR CONTROLLER WHEN SYSTEM FREQUENCY IS 49.1 HZ

Time	THD_is (%)	$P_{\_inj}$ (W)	P_{source} (W)	$Q_{\_inj}$ (var)	$Q_{\_load}$ (var)	$P_{\_error}$ (%)	$Q_{\_error}$ (%)
0.29 s	2.44	496.05	500	2084.51	2020.23	0.79	3.18
0.49 s	4.49	535.84	500	2831.69	2756.35	7.17	2.73
0.69 s	2.82	478.05	500	1307.92	1246.72	4.39	4.91

Moreover, the source current distortion is also lower. It can be concluded that the quasi-PR controller with carrier-based PWM is the better choice for use with the CGCI to achieve nearly zero steady-state current tracking errors.

C. Comparisons Between the PR Controller and the Quasi-PR Controller Under System Frequency Variations

A comparison between the PR controller and the quasi-PR controller are conducted. Both of these two controllers could reduce the steady-state current tracking error at fundamental frequency. The quasi-PR controller widens the bandwidth at the resonant frequency, as illustrated in Fig. 10. Therefore, their performance is compared under system frequency variations. The simulation results are listed in Tables VIII and IX when the system frequency is set to 49.1 Hz. Result indicates that

TABLE VIII
EXPERIMENTAL SYSTEM SETTINGS

Item	Value
Capacitor C_c	120.95 μF
Inductor L_c	3.791 μH
Grid voltage Vs	110 $V_{\rm rms}$, 50 Hz
DC-link voltage	85 V
Active power transfer	90 W
Linear load	14 Ω, 25.27 mH

TABLE IX
EXPERIMENTAL RESULTS

Time	THD_is (%)	$P_{\_inj}$ (W)	P_{source} (W)	$Q_{\_inj}$ (Kvar)	$Q_{\_load}$ (Kvar)	$P_{\_error}$ (%)	$Q_{\_error}$ (%)
PI	3.1	64	90	0.465	0.45	28.89	0.0333
PR	1.9	97	90	0.456	0.47	7.78	0.0298

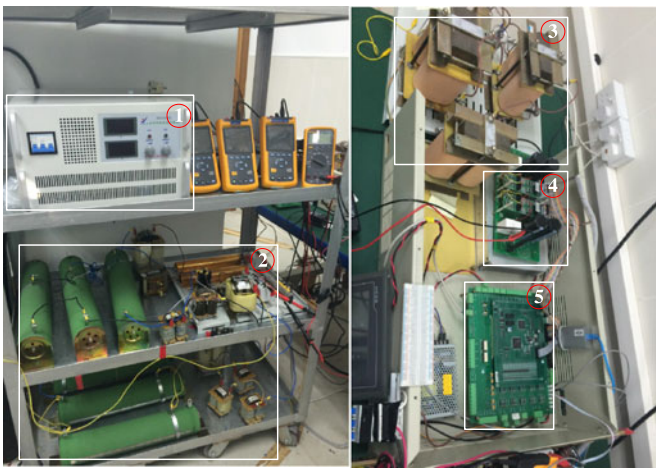

Fig. 15. Experimental prototype of a single-phase CGCI. ①DC power supply. ②Loads. ③Coupling impedance. ④IGBT and drivers. ⑤Control board and signal conditioning circuit.

the performance of the quasi-PR controller is slightly better under system frequency variation. Since the quasi-PR controller can provide sufficient gain in a wider band near the designed resonant frequency (50 Hz), it is selected to control the CGCI in this paper.

V. EXPERIMENTAL RESULTS

A single-phase CGCI experimental prototype was designed and constructed in the laboratory, and its system parameters are listed in Table VIII. The control algorithm is implemented in a DSP-TMS320F28335. A photo of the experimental prototype is shown in Fig. 15. The grid-side voltage is scaled down to 110 V due to limitations of the laboratory facilities.

The parameters of the quasi-PR controller ($K_p = 50, \omega_c = 5, K_r = 5800$) are designed according to the proposed parameter design procedures described in Section III. The experimental results of the CGCI are evaluated with the same performance parameters as used in the previous simulation case. The dc

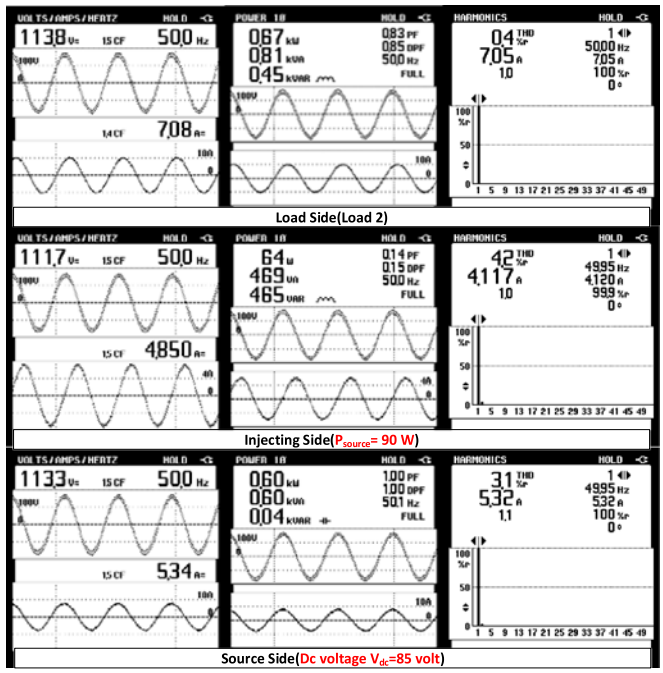

Fig. 16. Experimental results of the PI controller with carrier-based PWM.

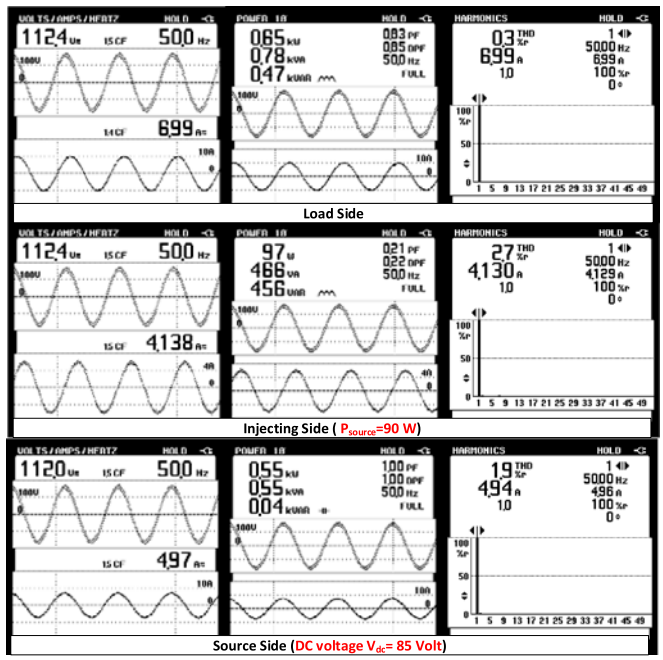

Fig. 17. Experimental results of the quasi-PR controller with carrier-based PWM

voltage is set to 85 V, which is lower than the grid-side voltage of 110 V. The active power reference is set at 90 W, and a linear inductive load is used.

Fig. 16 shows the experimental results (load-side, CGCI-side, and source-side results) when the PI controller with carrier-based PWM is used, and Fig. 17 shows the experimental results when the quasi-PR controller is applied in CGCI. The experimental results are summarized in Table IX. It can be concluded that the power tracking errors are greatly reduced when

the quasi-PR controller is used instead of the PI controller in CGCI. The source current distortion is also lower. The validity and effectiveness of the application the quasi-PR controller to be CGCI and its design method are thus proved.

VI. Conclusion

The CGCI can inject active power into the grid and compensate reactive power with an operational voltage lower than grid voltage. It is a promising alternative to a grid-connected inverter in a building-integrated distributed generator system or microgrid. The CGCI is coupled to the grid via a second-order *LC* branch. Therefore, the mathematical model and current controller for a traditional IGCI cannot be directly applied to the CGCI. A quasi-PR controller is applied to the CGCI to reduce the steady-state current tracking error. A corresponding control parameter design method is proposed. Both simulation and experimental results are provided to validate the proposed controller and its design. Comparison with a PI controller is also provided. The results show that the quasi-PR controller is the better choice to fulfill the requirements of active power and reactive power injection with low source current THD.

References

[1] V. K. N. Lau and D. H. K. Tsang, "Optimal energy scheduling for residential smart grid with centralized renewable energy source," *IEEE Syst. J.*, vol. 8, no. 2, pp. 562–576, Jun. 2014.

[2] C. K. Lee, B. Chaudhuri, and S. Y. Hui, "Hardware and control implementation of electric springs for stabilizing future smart grid with intermittent renewable energy sources," *IEEE J. Emerg. Sel. Topics Power Electron.*, vol. 1, no. 1, pp. 18–27, Mar. 2013.

[3] V. Salehi, A. Mohamed, A. Mazloomzadeh, and O. A. Mohammed, "Laboratory-based smart power system, part I: Design and system development," *IEEE Trans. Smart Grid*, vol. 3, no. 3, pp. 1394–1404, Sep. 2012.

[4] A. Izadian, N. Girrens, and P. Khayyer, "Renewable energy policies: A brief review of the latest U.S. and E.U. policies," *IEEE Ind. Electron. Mag.*, vol. 7, no. 3, pp. 21–34, Sep. 2013.

[5] H. Calleja and H. Jimenez, "Performance of a grid connected PV system used as active filter," *Energy Convers. Manage.*, vol. 45, nos. 15/16, pp. 2417–2428, Sep. 2004.

[6] Z. Zeng, H. Yang, R. Zhao, and C. Cheng, "Topologies and control strategies of multi-functional grid-connected inverters for power quality enhancement: A comprehensive review," *Renew. Sustain. Energy Rev.*, vol. 24, pp. 223–270, Aug. 2013.

[7] B. Hoff and W. Sulkowski, "Grid-connected VSI with LCL filter—Models and comparison," *IEEE Trans. Ind. Appl.*, vol. 50, no. 3, pp. 1974–1981, May 2014.

[8] A. Reznik, M. G. Simoes, A. Al-Durra, and S. M. Muyeen, "LCL filter design and performance analysis for grid-interconnected systems," *IEEE Trans. Ind. Appl.*, vol. 50, no. 2, pp. 1225–1232, Mar. 2014.

[9] X. Zhang, J. W. Spencer, and J. M. Guerrero, "Small-signal modeling of digitally controlled grid-connected inverters with LCL filters," *IEEE Trans. Ind. Electron.*, vol. 60, no. 9, pp. 3752–3765, Sep. 2013.

[10] W. Wu, Y. He, and F. Blaabjerg, "An LLCL power filter for single-phase grid-tied inverter," *IEEE Trans. Power Electron.*, vol. 27, no. 2, pp. 782–789, Feb. 2012.

[11] Z. Zou, Z. Wang, and M. Cheng, "Modeling, analysis, and design of multifunction grid-interfaced inverters with output LCL filter," *IEEE Trans. Power Electron.*, vol. 29, no. 7, pp. 3830–3839, Jul. 2014.

[12] W.-C. Zhang, N.-Y. Dai, and M.-C. Wong, "Capacitive-coupled grid-connected inverter with active power injection ability," in *Proc. 7th Int. Power Electron. Motion Control Conf.*, 2012, vol. 3, pp. 1639–1645.

[13] N.-Y. Dai, W.-C. Zhang, M.-C. Wong, J. M. Guerrero, and C.-S. Lam, "Analysis, control and experimental verification of a single-phase capacitive-coupling grid-connected inverter," *IET Power Electron.*, vol. 8, pp. 770–782, 2015.

[14] S. Srianthumrong and H. Akagi, "Medium-voltage transformerless ac/dc power conversion system consisting of a diode rectifier and a shunt hybrid filter," *IEEE Trans. Ind. Appl.*, vol. 39, no. 3, pp. 874–882, May 2003.

[15] R. Inzunza and H. Akagi, "A 6.6-kV transformerless shunt hybrid active filter for installation on a power distribution system," *IEEE Trans. Power Electron.*, vol. 20, no. 4, pp. 893–900, Jul. 2005.

[16] H. Akagi, "Active harmonic filters," *Proc. IEEE*, vol. 93, no. 12, pp. 2128–2141, Dec. 2005.

[17] S. Ostroznik, P. Bajec, and P. Zajec, "A study of a hybrid filter," *IEEE Trans. Ind. Electron.*, vol. 57, no. 3, pp. 935–942, Mar. 2010.

[18] C. S. Lam, M. C. Wong, and Y. D. Han, "Hysteresis current control of hybrid active power filters," *IET Power Electron.*, vol. 5, pp. 1175–1187, 2012.

[19] C.-S. Lam, W.-H. Choi, M.-C. Wong, and Y.-D. Han, "Adaptive DC-link voltage-controlled hybrid active power filters for reactive power compensation," *IEEE Trans. Power Electron.*, vol. 27, no. 4, pp. 1758–1772, Apr. 2012.

[20] C.-S. Lam and M.-C. Wong, *Design and Control of Hybrid Active Power Filter*. New York, NY, USA: Springer, Jan. 2014, pp. 39–60.

[21] W. Lei, L. Chi-Seng, and W. Man-Chung, "An adaptive hysteresis band controller for LC-coupling hybrid active power filter with approximate constant switching frequency," in *Proc. IEEE PES Asia-Pacific Power Energy Eng. Conf.*, 2014, pp. 1–5.

[22] Y. Li, D. M. Vilathgamuwa, and P. C. Loh, "Microgrid power quality enhancement using a three-phase four-wire grid-interfacing compensator," *IEEE Trans. Ind. Appl.*, vol. 41, no. 6, pp. 1707–1719, Nov. 2005.

[23] Y. Yang, H. Wang, and F. Blaabjerg, "Reactive power injection strategies for single-phase photovoltaic systems considering grid requirements," *IEEE Trans. Ind. Appl.*, vol. 50, no. 6, pp. 4065–4076, Nov. 2014.

[24] L. Herman, I. Papic, and B. Blazic, "A proportional-resonant current controller for selective harmonic compensation in a hybrid active power filter," *IEEE Trans. Power Del.*, vol. 29, no. 5, pp. 2055–2065, Oct. 2014.

[25] D. N. Zmood, D. G. Holmes, and G. H. Bode, "Frequency-domain analysis of three-phase linear current regulators," *IEEE Trans. Ind. Appl.*, vol. 37, no. 2, pp. 601–610, 2001.

[26] F. Blaabjerg, R. Teodorescu, M. Liserre, and A. V. Timbus, "Overview of control and grid synchronization for distributed power generation systems," *IEEE Trans. Ind. Electron.*, vol. 53, no. 5, pp. 1398–1409, Oct. 2006.

[27] S. Yang, Q. Lei, F. Z. Peng, and Z. Qian, "A robust control scheme for grid-connected voltage-source inverters," *IEEE Trans. Ind. Electron.*, vol. 58, no. 1, pp. 202–212, Jan. 2011.

[28] Z. Yao and L. Xiao, "Control of single-phase grid-connected inverters with nonlinear loads," *IEEE Trans. Ind. Electron.*, vol. 60, no. 4, pp. 1384–1389, Apr. 2013.

[29] M. P. Kazmierkowski and L. Malesani, "0043urrent control techniques for three-phase voltage-source PWM converters: A survey," *IEEE Trans. Ind. Electron.*, vol. 45, no. 5, pp. 691–703, Oct. 1998.

[30] F. Briz, M. Degner, and R. Lorenz, "Dynamic analysis of current regulators for AC motors using complex vectors," *IEEE Trans. Ind. Appl.*, vol. 35, no. 6, pp. 1424–1432, Nov./Dec. 1999.

[31] D. N. Zmood and D. G. Holmes, "Stationary frame current regulation of PWM inverters with zero steady-state error," *IEEE Trans. Power Electron.*, vol. 18, no. 3, pp. 814–822, May 2003.

[32] E. Twining and D. G. Holmes, "Grid current regulation of a three-phase voltage source inverter with an LCL input filter," *IEEE Trans. Power Electron.*, vol. 18, no. 3, pp. 888–895, May 2003.

[33] K. H. Ahmed, A. M. Massoud, S. J. Finney, and B. W. Williams, "A modified stationary reference frame-based predictive current control with zero steady-state error for LCL coupled inverter-based distributed generation systems," *IEEE Trans. Ind. Electron.*, vol. 58, no. 4, pp. 1359–1370, Apr. 2011.

[34] H. Lee and V. I. Utkin, "Chattering suppression methods in sliding mode control systems," *Annu. Rev. Control*, vol. 31, no. 2, pp. 179–188, 2007.

[35] T. Hornik and Q. C. Zhong, "A current-control strategy for voltage-source inverters in microgrids based on H ∞ and repetitive Control," *IEEE Trans. Power Electron.*, vol. 26, no. 3, pp. 943–952, Mar. 2011.

[36] F.-J. Chang, E.-C. Chang, T.-J. Liang, and J.-F. Chen, "Digital-signal-processor-based DC/AC inverter with integral-compensation terminal sliding-mode control," *IET Power Electron.*, vol. 4, no. 1, pp. 159–167, 2011.

[37] A. Abrishamifar, A. A. Ahmad, and M. Mohamadian, "Fixed switching frequency sliding mode control for single-phase unipolar inverters," *IEEE Trans. Power Electron.*, vol. 27, no. 5, pp. 2507–2514, May 2012.

[38] Y. Yang, K. Zhou, and W. Lu, "Robust repetitive control scheme for three-phase constant voltage constant frequency pulse width modulated inverters," *IET Power Electron*., vol. 5, no. 6, pp. 669–677, 2012.
[39] D. Chen, J. Zhang, Z. Qian, and S. Member, "An improved repetitive control scheme for grid-connected inverter with frequency-adaptive capability," *IEEE Trans. Ind. Electron.*, vol. 60, no. 2, pp. 814–823, 2013.
[40] J. Hu, J. Zhu, and D. G. Dorrell, "Model predictive control of grid-connected inverters for PV systems with flexible power regulation and switching frequency reduction," *IEEE Trans. Ind. Appl.*, vol. 51, no. 1, pp. 587–594, Jan./Feb. 2015.
[41] M. P. Kazmierkowski and L. Malesani, "Current control techniques for three-phase voltage-source PWM converters: A survey," *IEEE Trans. Ind. Electron.*, vol. 45, no. 5, pp. 691–703, Oct. 1998.
[42] A Bhattacharya and C. Chakraborty, "A shunt active power filter with enhanced performance using ANN-based predictive and adaptive controllers," *IEEE Trans. Ind. Electron.*, vol. 58, no. 2, pp. 421–428, Feb. 2011.
[43] C. W. Tao, C. M. Wang, and C. W. Chang, "A design of a dc-ac inverter using a modified ZVS-PWM auxiliary commutation pole and a DSP-based PID-like fuzzy control," *IEEE Trans. Ind. Electron.*, vol. 63, no. 1, pp. 397-405, Jan. 2016 .
[44] D. P. F. Control, C. Tao, S. Member, and C. Wang, "A design of a dc–ac inverter using a modified ZVS-PWM auxiliary commutation pole and a DSP-based PID-like fuzzy control," vol. 63, no. 1, pp. 397–405, Jan. 2016.
[45] J. M. Guerrero, J. Matas, L. Garcia de Vicuna, N. Berbel, and J. Sosa, "Wireless-control strategy for parallel operation of distributed generation inverters," in *Proc. IEEE Int. Symp. Ind. Electron.*, 2005, vol. 2, pp. 845–850.
[46] D. M. Van de Sype, K. De Gusseme, A. P. Van den Bossche, and J. A. Melkebeek, "Small-signal Laplace-domain analysis of uniformly-sampled pulse-width modulators," in *Proc. IEEE 35th Annu. Power Electron. Spec. Conf.*, 2004, vol. 6, pp. 4292–4298.
[47] D. Maksimovic and R. Zane, "Small-signal discrete-time modeling of digitally controlled PWM converters," *IEEE Trans. Power Electron.*, vol. 22, no. 6, pp. 2552–2556, Nov. 2007.
[48] P. Geng, W. Wu, Y. Ye, and Y. Liu, "Small signal modeling of a novel single-phase photovoltaic inverter," in *Proc. IEEE 6th Int. Power Electron. Motion Control Conf.*, 2009, pp. 2188–2192.
[49] B.-H. Bae and S.-K. Sul, "A compensation method for time delay of full digital synchronous frame current regulator of PWM AC drives," in *Proc. IEEE 36th Conf. Rec. Ind. Appl. Conf. Annu. Meeting*, 2001, vol. 3, pp. 1708–1714.
[50] D. G. Holmes, T. A. Lipo, B. P. McGrath, and W. Y. Kong, "Optimized design of stationary frame three phase AC current regulators," *IEEE Trans. Power Electron.*, vol. 24, no. 11, pp. 2417–2426, Nov. 2009.
[51] D. G. Holmes, B. P. McGrath, and S. G. Parker, "Current regulation strategies for vector-controlled induction motor drives," *IEEE Trans. Ind. Electron.*, vol. 59, no. 10, pp. 3680–3689, Oct. 2012.
[52] A. G. Yepes, A. Vidal, J. Malvar, O. Lopez, and J. Doval-Gandoy, "Tuning method aimed at optimized settling time and overshoot for synchronous proportional-integral current control in electric machines," *IEEE Trans. Power Electron.*, vol. 29, no. 6, pp. 3041–3054, Jun. 2014.
[53] A. Khairy, M. Ibrahim, N. Abdel-Rahim, and H. Elsherif, "Comparing proportional-resonant and fuzzy-logic controllers for current controlled single-phase grid-connected PWM DC/AC Inverters," in *Proc. IET Conf. Renew. Power Gener.*, 2011, pp. 153–153.
[54] D. N. Zmood and D. G. Holmes, "Stationary frame current regulation of PWM inverters with zero steady state error," in *Proc. IEEE 30th Annu. IEEE Power Electron. Spec. Conf. Rec.*, 1999, vol. 2, pp. 1185–1190.
[55] R. Teodorescu, F. Blaabjerg, M. Liserre, and P. C. Loh, "Proportional-resonant controllers and filters for grid-connected voltage-source converters," *IEE Proc. Elect. Power Appl.*, vol. 153, no. 5, pp. 750–762, Sep. 2006.
[56] A. Micallef, M. Apap, C. Spiteri-Staines, J. M. Guerrero, and J. C. Vasquez, "Reactive power sharing and voltage harmonic distortion compensation of droop controlled single phase islanded microgrids," *IEEE Trans. Smart Grid*, vol. 5, no. 3, pp. 1149–1158, May 2014.
[57] CEM-Companhia de Electricidade de Macau, "Electricity supply," [Online]. Available: http://www.cem-macau.com/Electricity-Supply. Accessed on: 2015.
[58] CPL Power Hong Kong Limited, "Supply rules," Hong Kong. [Online]. Available: https://www.clp.com.hk/zh/customer-service/open-and-close-account/supply-rules. Accessed on: 2015.

Tao Ye received the B.Sc. degree in electronic and information engineering from the Wuhan University of Science and Technology, Hubei, China, in 2013, and the M.Sc. degree in electrical and computer engineering from the University of Macau, Macao SAR, China, in 2016.

His research interest includes grid-connected inverter and renewable energy integration.

NingYi Dai (S'05–M'08–SM' 15) received the B.Sc. degree in electrical engineering from Southeast University, Nanjing, China, in 2001, and the M.Sc. and Ph.D. degrees in electrical and electronics engineering from the Faculty of Science and Technology, University of Macau, Macao, China, in 2004 and 2007, respectively.

She is currently an Assistant Professor with the Department of Electrical and Computer Engineering, University of Macau. She has published more than 60 technical journals and conference papers in the field of power system and power electronics. Her research interests include application of power electronics in power system, renewable energy integration, and pulse-width modulation.

Dr. Dai received the Macao Science and Technology Invention Award (Third-Class) in 2012.

Chi-Seng Lam (S'04–M'12–SM'16) received the B.Sc., M.Sc., and Ph.D. degrees in electrical and electronics engineering from the University of Macau (UM), Macao, China, in 2003, 2006, and 2012, respectively.

From 2006 to 2009, he was an Electrical and Maintenance Engineer at UM. In 2009, he simultaneously worked as a Laboratory Technician and started to pursue his Ph.D. degree, and completed his Ph.D. within three years. In 2013, he was a Post-Doctoral Fellow at Hong Kong Polytechnic University, Hong Kong, China. He is currently an Assistant Professor with the State Key Laboratory of Analog and Mixed-Signal VLSI, UM. He has co-authored the two books *Design and Control of Hybrid Active Power Filters* (Springer, 2014) and *Parallel Power Electronics Filters in Three-Phase Four-Wire Systems—Principle, Control, and Design* (Springer, in press), one U.S. patent, two Chinese patents, and more than 50 technical journals and conference papers. His research interests include integrated power electronics controllers, power management integrated circuits, power quality compensators, smart grid technology, renewable energy, etc.

Dr. Lam received the Macao Science and Technology Invention Award (Third Class) and the Research and Development Award for Post-Graduates (Ph.D.) in 2014 and 2012, respectively. He also received the Macao Government Ph.D. Research Scholarship in 2009–2012, the Macao Foundation Post-Graduate Research Scholarship in 2003–2005, and the 3rd Regional Inter-University Post-Graduate Electrical and Electronic Engineering Conference Merit Paper Award in 2005. In 2007, 2008, and 2015, he was the GOLD Officer, Student Branch Officer, and Secretary of the IEEE Macau Section. He is currently the Vice Chair of the IEEE Macau Section and Secretary of the IEEE Macau Power and Energy Society and the Power Electronics Society Joint Chapter. He was the Local Arrangement Chair of TENCON 2015 and Asia and the South Pacific Design Automation Conference 2016.

Man-Chung Wong (SM'06) received the B.Sc. and M.Sc. degrees in electrical and electronics engineering from the Department of Electrical and Electronics Engineering, University of Macau, Macau, China, in 1993 and 1997, respectively, and the Ph.D. degree from Tsinghua University, Beijing, China, in 2003.

He was a Visiting Fellow (July–Dec. 2014) at Cambridge University, Cambridge, U.K. He is currently an Associate Professor with the Department of Electrical and Computer Engineering, University of Macau. He has published more than 100 journal and conference papers. His current research interests include flexible ac transmission system and distribution flexible ac transmission system, power quality, custom power, and pulse-width modulation.

Dr. Wong received the Young Scientist Award from the Instituto Internacional De Macau, Macau, in 2000; the Young Scholar Award from the University of Macau in 2001, the Second Prize Excellent Doctor Thesis Award from Tsinghua University, Beijing, China, in 2003; the Third Prize Invention Awards from Macau Government Science and Development 2012 and 2014, respectively.

Josep M. Guerrero (S'01–M'04–SM'08–F'15) received the B.S. degree in telecommunications engineering, the M.S. degree in electronics engineering, and the Ph.D. degree in power electronics from the Technical University of Catalonia, Barcelona, Spain, in 1997, 2000, and 2003, respectively.

Since 2011, he has been a Full Professor with the Department of Energy Technology, Aalborg University, Aalborg, Denmark, where he is responsible for the Microgrid Research Program. Since 2012, he has been a Guest Professor with the Chinese Academy of Science and the Nanjing University of Aeronautics and Astronautics P. R. China. Since 2014, he has been the Chair Professor with Shandong University. Since 2015, he has been a Distinguished Guest Professor with Hunan University. Since 2016, he has been a Visiting Professor Fellow with Aston University, Birmingham, U.K. His research interests include different microgrid aspects, including power electronics, distributed energy-storage systems, hierarchical and cooperative control, energy management systems, smart metering, and the Internet of things for ac/dc microgrid clusters and islanded minigrids; recently, he has especially focused on maritime microgrids for electrical ships, vessels, ferries, and seaports.

Prof. Guerrero is an Associate Editor for the IEEE TRANSACTIONS ON POWER ELECTRONICS, the IEEE TRANSACTIONS ON INDUSTRIAL ELECTRONICS, and the IEEE INDUSTRIAL ELECTRONICS MAGAZINE, and an Editor for the IEEE TRANSACTIONS ON SMART GRID and the IEEE TRANSACTIONS ON ENERGY CONVERSION. He has been the Guest Editor of the IEEE TRANSACTIONS ON POWER ELECTRONICS Special Issues on Power Electronics for Wind Energy Conversion and Power Electronics for Microgrids; the IEEE TRANSACTIONS ON INDUSTRIAL ELECTRONICS Special Sections on Uninterruptible Power Supplies Systems, Renewable Energy Systems, Distributed Generation, and Microgrids, and Industrial Applications and Implementation Issues of the Kalman Filter; the IEEE TRANSACTIONS ON SMART GRID Special Issues on Smart DC Distribution Systems and Power Quality in Smart Grids and the IEEE TRANSACTIONS ON ENERGY CONVERSION Special Issue on Energy Conversion in Next-Generation Electric Ships. He was the Chair of the Renewable Energy Systems Technical Committee of the IEEE Industrial Electronics Society. He received the Best Paper Award of the IEEE TRANSACTIONS ON ENERGY CONVERSION for the 2014–2015. In 2014 and 2015, he was awarded by Thomson Reuters as a Highly Cited Researcher, and in 2015 he was elevated as an IEEE Fellow for his contributions on distributed power systems and microgrids.